Combination of irinotecan silicasome nanoparticles with radiation therapy sensitizes immunotherapy by modulating the activation of the cGAS/STING pathway for colorectal cancer

Lu Wang [a,b,1], Tianyu Zhang [a,c,1], Yile Zheng [a,c], Yuting Li [a], Xiyuan Tang [a,b], Qianping Chen [a,b], Wei Mao [a,b], Weiwei Li [a,b], Xiangsheng Liu [a,b,**], Ji Zhu [a,b,*]

[a] Zhejiang Cancer Hospital, Hangzhou Institute of Medicine (HIM), Chinese Academy of Sciences, Hangzhou, Zhejiang, 310022, China
[b] Zhejiang Key Laboratory of Radiation Oncology, Hangzhou, Zhejiang, 310022, China
[c] Shanghai Institute of Materia Medica, Chinese Academy of Sciences, Shanghai, 201203, China

A B S T R A C T

Our previous clinical trial (Identifier: NCT02605265) revealed that addition of irinotecan (IRIN) to neoadjuvant chemoradiotherapy for rectal cancer could improve the curative effect. However, the adverse effects caused by IRIN limited the wide application of IRIN chemoradiotherapy. This study aimed to explore the mechanism under the synergistic effects of IRIN plus radiation therapy in colorectal cancer (CRC) cells and optimization of IRIN delivery via a silicasome nanocarrier *in vivo*. Our results revealed that compared with single IRIN or radiation treatment, IRIN combined with radiation therapy remarkably activated the intracellular cGAS/STING pathway, and promoted the expression levels of major histocompatibility complex class I (MHC-I) and programmed death ligand 1 (PD-L1). Further, a silicasome (mesoporous silica nanoparticle coated with lipid bilayer) nanocarrier was utilized to improve the delivery of IRIN with enhanced efficacy and reduced side effects. In the MC38 CRC syngeneic tumor model, IRIN silicasome combined with radiation therapy demonstrated a greater antitumor efficacy than free IRIN plus radiation therapy. Flow cytometry showed the increased number of CD4+ T cells, CD8+ T cells, and dendritic cells (DCs) in tumor in the IRIN silicasome plus radiation group. The immunofluorescence staining further confirmed the activated immune microenvironment with the elevated interferon-γ (IFN-γ) deposition. Besides, the antitumor effect of IRIN silicasome plus radiation therapy was synergistically enhanced by *anti*-PD-1 immunotherapy. These findings indicated that the combination of IRIN silicasome with radiation therapy could sensitize immunotherapy by manipulating the cGAS/STING pathway serving as a new strategy for CRC treatment.

1. Introduction

According to the statistics released by the American Cancer Society, the new incidence rate of colorectal cancer (CRC) will rank fourth among all types of cancer in 2023, accounting for approximately 153,000 cases. The mortality rate will rank second, accounting for approximately 53,000 deaths [1]. For locally advanced (T3-4/N + M0) rectal cancer (LARC), fluorouracil-based neoadjuvant chemoradiotherapy (nCRT), followed by total mesorectal excision (TME) is the standard of care [2]. It can reduce the local recurrence rate of tumors. Some patients could achieve pathologic complete remission (pCR), whose prognosis was better than that of patients who could not achieve pCR. Clinically, patients who achieved clinical complete remission (cCR) could benefit from a watch-and-wait strategy to preserve organ

function and obtain a better quality of life [3]. However, only 10–15% of patients could achieve pCR, and the distant metastasis rate was >30% [4]. The 5-year survival rate of metastatic CRC was only about 15% [5]. The increasing demand for tumor regression and organ function preservation has challenged the traditional nCRT treatment modalities. How to increase the pCR and reduce the rate of distant metastasis is an urgent problem to be solved.

To date, few studies demonstrated that the application of systemic chemotherapy in nCRT can reduce local recurrence and distant metastasis in patients. Several attempts have been made regarding the optimization of chemotherapy regimens in nCRT. Irinotecan (IRIN) is a very important chemotherapeutic drug for the treatment of CRC, pancreatic cancer, and lung cancer. The addition of IRIN to nCRT for rectal cancer has been initially explored in several previous clinical trials [6–13]. The

---

* Corresponding author. Professor. Zhejiang Cancer Hospital, Hangzhou Institute of Medicine (HIM), Chinese Academy of Sciences, Banshan Road 1, Gongshu District, Hangzhou, 310022, China.
** Corresponding author. Zhejiang Cancer Hospital, Hangzhou Institute of Medicine (HIM), Chinese Academy of Sciences, Banshan Road 1, Gongshu District, Hangzhou, 310022, China.
E-mail addresses: xsliu@zju.edu.cn (X. Liu), zhuji@zjcc.org.cn (J. Zhu).
[1] These authors are co-first authors of the study.

clinical application of IRIN is limited by its adverse reactions, such as diarrhea and neutropenia. As a result, it is difficult to increase its dose, which in turn leads to a limited efficacy. The uridine diphospho-glucuronate-glucuronosyltransferase 1A1 (UGT1A1) is the metabolizing enzyme of IRIN. Its mutation status can affect the toxicity of IRIN *in vivo* [14,15]. Our team previously designed a phase III clinical trial, in which IRIN was added to the original fluorouracil-based nCRT. We individually designed the dose of IRIN according to the patient's UGT1A1 genotype [16]. The results suggested that compared with fluorouracil-based nCRT, addition of IRIN to nCRT significantly improved patients' pCR rate. However, addition of IRIN also caused a significant increase in grade 3-4 adverse reactions. Therefore, how to further optimize the administration of IRIN to enhance its tumor killing effect and reduce its adverse reactions is of great significance.

Immunotherapy has made remarkable progress in the treatment of CRC in recent years. Patients with high-microsatellite instability (MSI-H) have a higher tumor mutational burden (TMB), and they are sensitive to immunotherapy [17,18]. The Keynote-177 study demonstrated that pembrolizumab monotherapy could be used as a standard first-line treatment for patients with metastatic deficient mismatch repair (dMMR)/MSI-H CRC [19]. Nevertheless, the response rate of immunotherapy in non-dMMR patients was very low [20]. Therefore, it is essential to further assess the effects of immunotherapy on CRC patients. The addition of immunotherapy to nCRT is currently being explored clinically. Clinicians attempted to make the tumor microenvironment "hot" by designing different regimens including radiotherapy and chemotherapy, so as to increase the responsiveness of immunotherapy and further improve the efficacy of neoadjuvant therapy. Numerous preclinical studies have shown that activation of the cyclic GMP–AMP synthase (cGAS)–stimulator of interferon genes (cGAS/STING) pathway in tumor cells is an effective method to activate the tumor immune microenvironment (TIME) [21]. Radiation and chemotherapeutic drugs can damage nuclear DNA, resulting in the accumulation of double-stranded DNA (dsDNA) and micronuclei in the cytoplasm. The binding of dsDNA to cGAS triggers the production of the second messenger cGAMP [22], which further binds to STING inducing the production of type-I interferon (IFN) [23]. Studies also showed the activation of the cGAS/STING pathway in tumor cells *in vivo* can activate immune cells in the tumor microenvironment [24,25], making it possible to increase the sensitivity of immunotherapy. Therefore, it is essential to indicate whether the combination of IRIN with radiation therapy could trigger the cGAS/STING pathway and activate the tumor microenvironment of CRC.

Our previous study demonstrated that IRIN silicasome improved IRIN delivery compared with IRIN liposomes and free drug in orthotopic colorectal and pancreatic cancer models. The use of IRIN silicasome improved tumor control, while reduced intestinal and bone marrow toxicity [26]. Moreover, we also found that IRIN silicasome is immunogenic in pancreatic cancer and can activate the TIME [27]. Radiation therapy can damage tumor vascular endothelial cells and increase vascular permeability, which is conducive to the delivery of nanomedicine [28]. This stimulates scholars to clarify whether IRIN silicasome combined with radiation therapy can achieve a superior therapeutic efficacy than the free drug plus radiation therapy *in vivo*. In the present study, a synergistic effect between free IRIN and radiation therapy was first explored at the cellular level by promoting the apoptosis, and the combination that could activate the cGAS/STING pathway of tumor cells was assessed. It was revealed that IRIN silicasome could achieve a greater antitumor efficacy than free drug when combined with radiation therapy *in vivo*, and it could activate the TIME, providing the basis for further combination with anti-programmed cell death protein 1 (PD-1) immunotherapy.

2. Results

2.1. Synergistic effects of the combination of IRIN with radiation therapy

According to our clinical trial [16], addition of IRIN to nCRT significantly improved patients' pCR rate. Hence, it was attempted to indicate whether the combination of IRIN with radiation therapy could have a synergistic effect at the mechanism level. Radiation therapy causes DNA damage through the direct and indirect effects, mainly acting on cells in the G2/M phase, while cells in the S phase are resistant to radiation therapy [29]. Notably, IRIN is an inhibitor of topoisomerase I, mainly killing cells in the S phase [30]. Theoretically, there is a synergistic effect between IRIN and radiation therapy. Firstly, two CRC cell lines (HCT8 and HT29) were investigated for the sensitivity of IRIN when pretreated with radiation therapy. Briefly, cells were irradiated with 2 Gy X-rays which had mild effect on cell survival based on our experimental experience, and they were then treated with different concentrations of IRIN. After 48 h, the cell counting kit-8 (CCK-8) assay was used to detect the cell viability. The half maximal inhibitory concentration (IC$_{50}$) results showed that radiation pretreatment could increase the sensitivity of tumor cells to IRIN (Fig. 1A and B). In the colony formation assay, 1 μM IRIN was used to pretreat tumor cells for 12 h. After withdrawing the drug, the cells were exposed to 0, 2, 4, and 6 Gy X-rays. The colony formation ability of cells treated with IRIN was significantly lower than that of non-IRIN group, and the sensitizer enhancement ratio (SER) was 1.25, indicating that IRIN could sensitize CRC cells to radiation therapy (Fig. 1C).

As the reactive oxygen species (ROS) generated by radiation therapy is one of the important factors leading to DNA damage [31], the fluorescent probe DCFH-DA was further utilized to identify the production of ROS in the control group, IRIN group (3 μM), radiation group (4 Gy X-rays), and IRIN (3 μM) plus radiation (4 Gy X-rays) group (Fig. 1D). The production of ROS in the IRIN plus radiation group was significantly higher than that in the other three groups ($P < 0.05$) (Fig. 1E). Subsequently, Annexin V and PI staining was employed to detect the apoptosis rate in the four groups. The results revealed that the IRIN plus radiation group had higher rates of both early (annexin V+, PI-) and late (annexin V+, PI+) apoptotic cells compared with the other three groups ($P < 0.05$) (Fig. 1F and G). The Bliss synergy scoring system [32,33] was utilized to assess the effects of two drug combinations, which showed that the combination of IRIN and radiation therapy had a synergistic effect on the cell death (Fig. 1H).

2.2. IRIN combined with radiation therapy strongly damaged DNA and activated the cGAS/STING pathway

DNA damage due to radiation therapy or chemotherapy could induce the accumulation of abnormal dsDNA fragments, which was closely associated with the activation of the cGAS/STING pathway [34]. In addition, abnormal replication and division of chromatin could lead to the generation of micronuclei, which could also activate the cGAS/STING-dependent type-I IFN pathway [35,36]. To investigate the DNA damage and activation of the cGAS/STING pathway caused by the combination of IRIN and radiation therapy, the foci of the DNA damage marker r-H2AX in HT29 cells were detected (Fig. 2A). In the radiation group, cells were irradiated by 4 Gy X-ray, and r-H2AX was detected 24 h after radiation therapy. In the IRIN group, the cells were treated with 3 μM IRIN for 36 h. In the IRIN plus radiation group, cells received 4 Gy X-rays after 12 h of IRIN pretreatment. The results showed that the number of r-H2AX foci was higher in the IRIN plus radiation group compared with the other three groups ($P < 0.05$), suggesting that DNA damage was more severe in the combined treatment group. (Fig. 2B). Similar results were also found in HCT8 cells (Figs. S1A–B).

In addition, dsDNA was detected in the four treatment groups in HT29 and HCT8 cells (Fig. 2C, Figs. S1C–D). The results revealed that the IRIN plus radiation group had more dsDNA in the cytoplasm
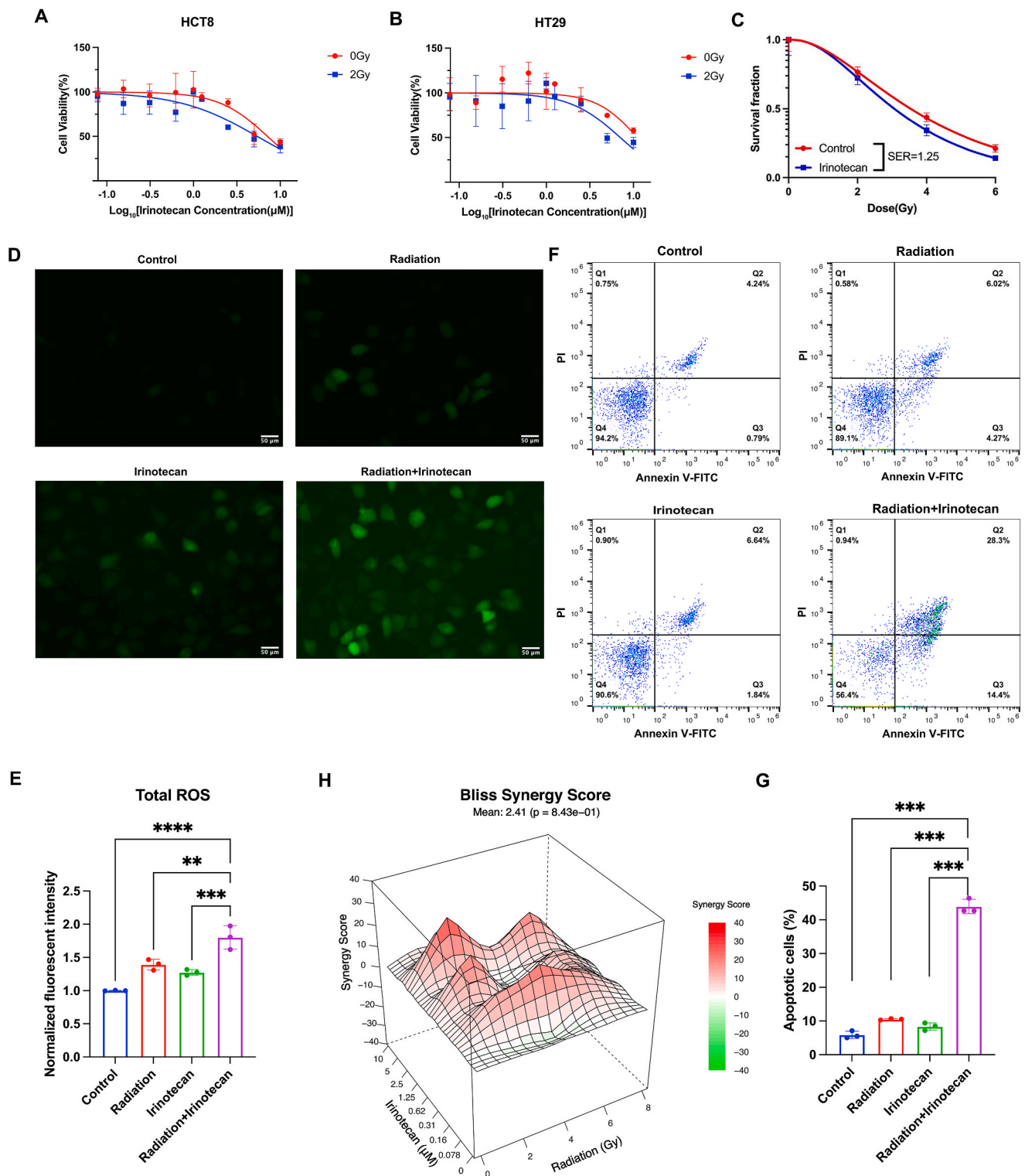
Fig. 1. Synergistic effects of the combination of IRIN with radiation therapy. (A–B) The IC$_{50}$ of IRIN in HCT8 (A) and HT29 (B) cells exposed to X-ray 0 Gy (red) and 2 Gy (blue). (C) Dose responses of the survival fractions of HCT8 cells treated with (blue) and without (red) IRIN (1 μM). SER = 1.25. (D) Representative fluorescence microscopy demonstrating ROS production in HCT8 cells with different treatments. Intracellular ROS level was evaluated by the fluorescent probe DCFH-DA. Green: ROS-positive cells. Bar: 50 μm. (E) Fluorescence quantitation of ROS measurement. Fluorescent intensity was quantified by ImageJ software. Data were presented as mean ± SD. At least three representative images were analyzed for each treatment. (F) Flow cytometry of apoptosis of HCT8 cells exposing to different treatments. Annexin V and PI staining was used to identify viable cells (annexin V$^-$, PI$^-$), early apoptotic cells (annexin V$^+$, PI$^-$), late apoptotic or necrotic cells (annexin V$^+$, PI$^+$), and necrotic cells (annexin V$^-$, PI$^+$). (G) Percentage of apoptotic cells analyzed from (F). Data were presented as mean ± SD, n = 3. (H) The synergistic effect of radiation therapy and IRIN on HCT8 cells. Corresponding to each treatment (x-axis and y-axis), the Bliss synergy score was presented on the z-axis. *$P < 0.05$, **$P < 0.01$, ***$P < 0.001$ (One-way ANOVA, followed by Tukey's test). (For interpretation of the references to colour in this figure legend, the reader is referred to the Web version of this article.)
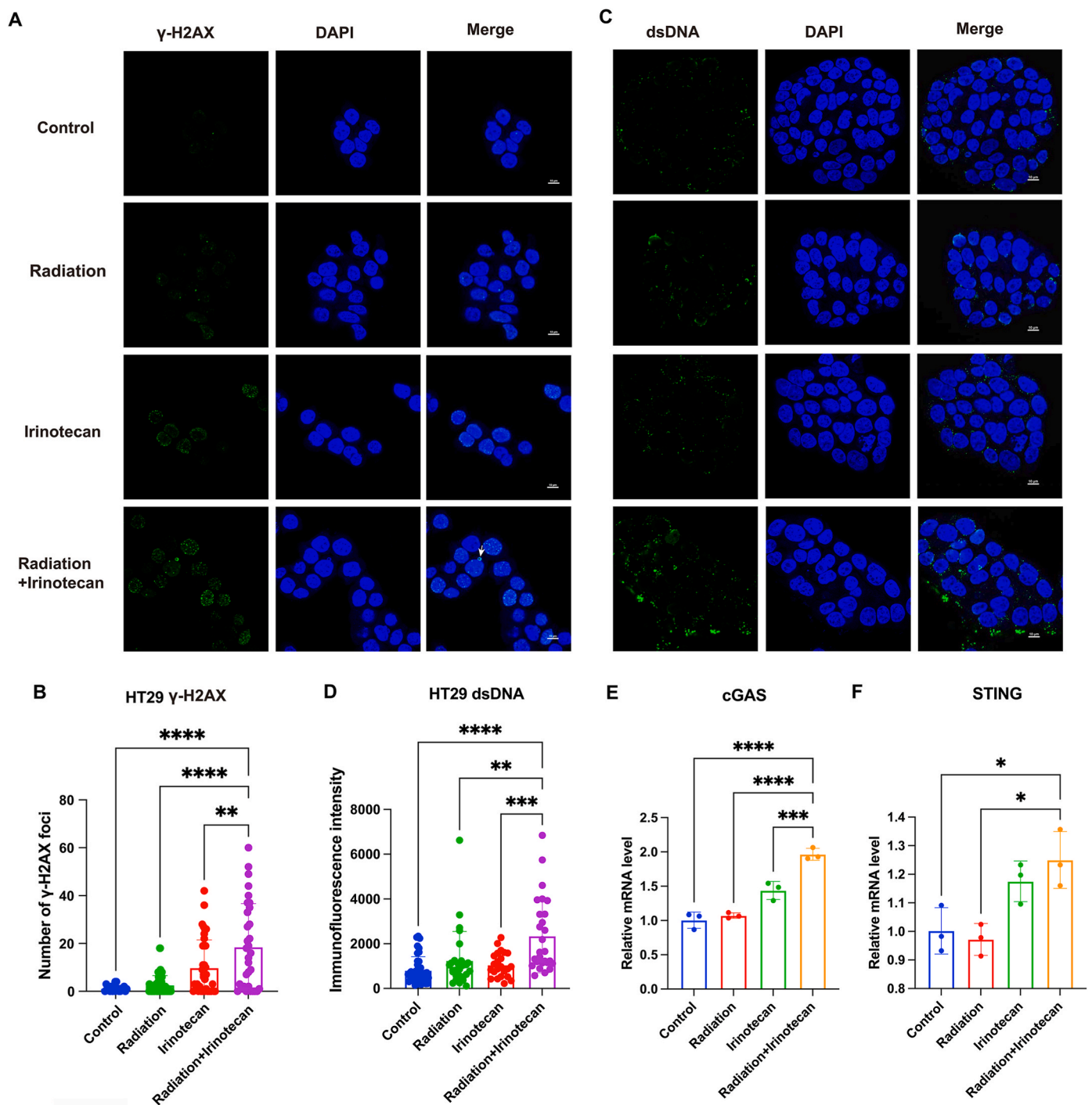
Fig. 2. IRIN plus radiation therapy strongly damaged DNA and activated the cGAS/STING pathway (A) Representative confocal laser scanning microscopic images of nuclear γ-H2AX foci in HT29 cells with different treatments. Green: γ-H2AX. Blue: DAPI. White arrow: micronuclei. Bar: 10 μm. (B) Quantitation of the number of γ-H2AX foci in (A). Data were presented as the mean ± SD obtained from three independent experiments. (C) Representative confocal laser scanning microscopic images of dsDNA in HT29 cells with different treatments. Green: dsDNA. Blue: DAPI. Bar: 10 μm. (D) Quantitation of fluorescent intensity of dsDNA in (C). Data were presented as the mean ± SD obtained from three independent experiments. (E–F) qRT-PCR analysis of cGAS (E) and STING (F) expression levels in HCT8 cells with different treatments. Data were presented as the mean ± SD obtained from three independent experiments. (G) Western blot analysis and quantitation of cGAS/STING pathway-related proteins in HCT8 cells with different treatments. ImageJ software was used for densitometric analysis. *$P < 0.05$, **$P < 0.01$, ***$P < 0.001$, ****$P < 0.0001$ (One-way ANOVA, followed by Tukey's test). (For interpretation of the references to colour in this figure legend, the reader is referred to the Web version of this article.)

compared with the other treatment groups ($P < 0.05$) (Fig. 2D). Moreover, there was a higher production of micronuclei in the combined treatment group. The results of qRT-PCR indicated that the mRNA levels of cGAS and STING were higher in the combined treatment group than

those in the other three groups in HCT8 cells (Fig. 2E and F). Western blotting of HCT8 cells further confirmed the abovementioned results (Fig. 2G). In the combined treatment group, the protein expression levels of cGAS, p-IRF3, and p-TBK1 were remarkably higher than those
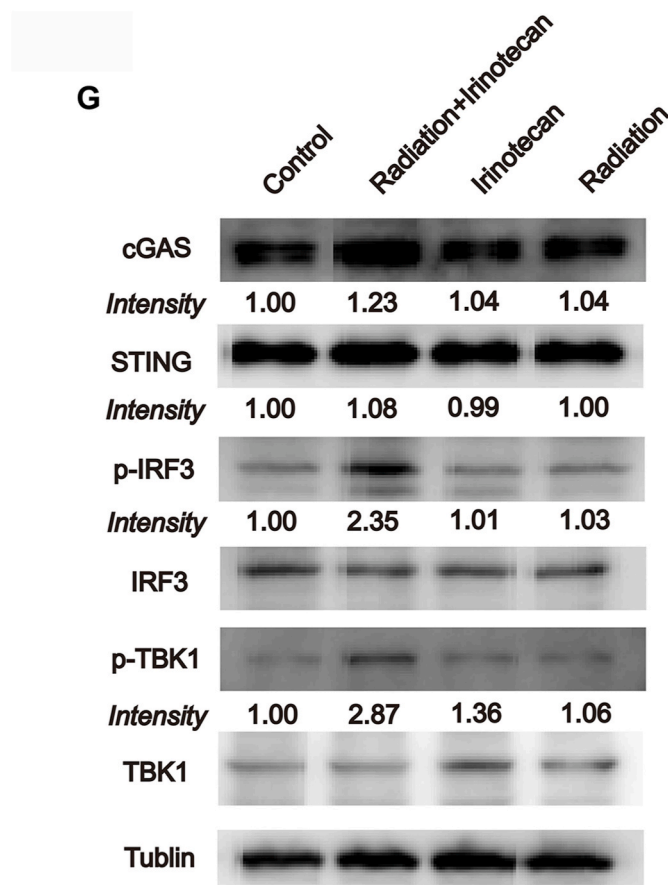
Fig. 2. (*continued*).

in the control, IRIN, and radiation groups. Taken together, these data suggested that the combination of IRIN and radiation therapy could activate the cGAS/STING-dependent type I IFN pathway.

2.3. IRIN combined with radiation therapy significantly increased antigen presentation and PD-L1 expression level in CRC cells

Activation of type I IFN can increase tumor cell antigen presentation and upregulate major histocompatibility complex class I (MHC-I) expression level. Antigen presentation is crucial for T cell recognition, killing and tumor immunity activation [37,38]. It was reported that radiation therapy and chemotherapy could not only increase MHC-I expression level, but also upregulate programmed death ligand 1 (PD-L1) expression level [39]. The overexpression of PD-L1 may induce tumor-immune tolerance. However, this provides an opportunity for *anti*-PD-1 and *anti*-PD-L1 therapy [40]. In the present study, flow cytometry was used to detect the expression levels of MHC-I and PD-L1 on the surface of HCT8 cells subjected to four different treatments (control, radiation, IRIN, and the combined treatment groups). The results demonstrated that the combined treatment remarkably upregulated the expression levels of PD-L1 (Fig. 3A and B) and MHC-I (Fig. 3C and D) compared with single treatment or negative control groups. Furthermore, qRT-PCR assay confirmed that the mRNA levels of type I IFN, including IFN-α and IFN-β, were risen in the combined treatment group (Fig. 3E and F). Additionally, mRNA level of ISG15, a gene induced by IRF3 in the downstream of the cGAS/STING pathway [41], increased (Fig. 3G). The ELISA results of IFN-α and IFN-β also confirmed the same trend (Fig. 3H and I). The expression levels of nucleotide-binding oligomerization domain-like receptor family caspase recruitment domain containing 5 (NLRC5), a gene that could upregulate MHC-I expression level [42,43], and transporter associated with antigen

processing 1 (TAP1), which is related to antigen processing [44], were also upregulated in the combined treatment group (Fig. 3J and K). The results of western blotting showed a higher expression level of β2 microglobulin (β2M), a component of MHC-I, in the combined treatment group (Fig. 3L). In summary, the combined treatment could significantly activate antigen presentation and processing pathways, providing potential opportunities to enhance the effects of immunotherapy.

2.4. The role of activation of the cGAS/STING activation in radiation therapy plus IRIN when delivered by a silicasome nanocarrier

Radiation therapy combined with free IRIN can effectively induce cell death, activate the cGAS/STING pathway, and increase antigen presentation *in vitro*. Nevertheless, the *in vivo* efficacy of free IRIN is still limited by its systemic toxicity, including severe diarrhea and leukopenia. The establishment of a more efficient drug delivery system can improve the tumor control while decreasing the adverse effects. Compared with IRIN free drug, IRIN liposome Onivyde was more effective in tumor control and reduced the adverse reactions of the drug [45]. In our laboratory, we have previously established IRIN silicasome nanocarrier consisting of IRIN encapsulated within a mesoporous silica core, which is surrounded by a lipid bilayer on the outside (Fig. 4A). We found that compared with IRIN liposome, IRIN silicasome had a better stability, a longer blood circulation time, a lower toxicity, and a greater tumor control [26]. In the present study, it was attempted to further investigate whether combination of IRIN silicasome with radiation therapy could lead to a more robust synergistic effect for CRC treatment.

The IRIN silicasome was prepared based our previous protocol [26], and demonstrated similar physicochemical characteristics with of a particle size of approximately 111.6 nm, a slight negative charge, and a drug loading capacity of ~40% (Fig. 4B). In order to explore whether the
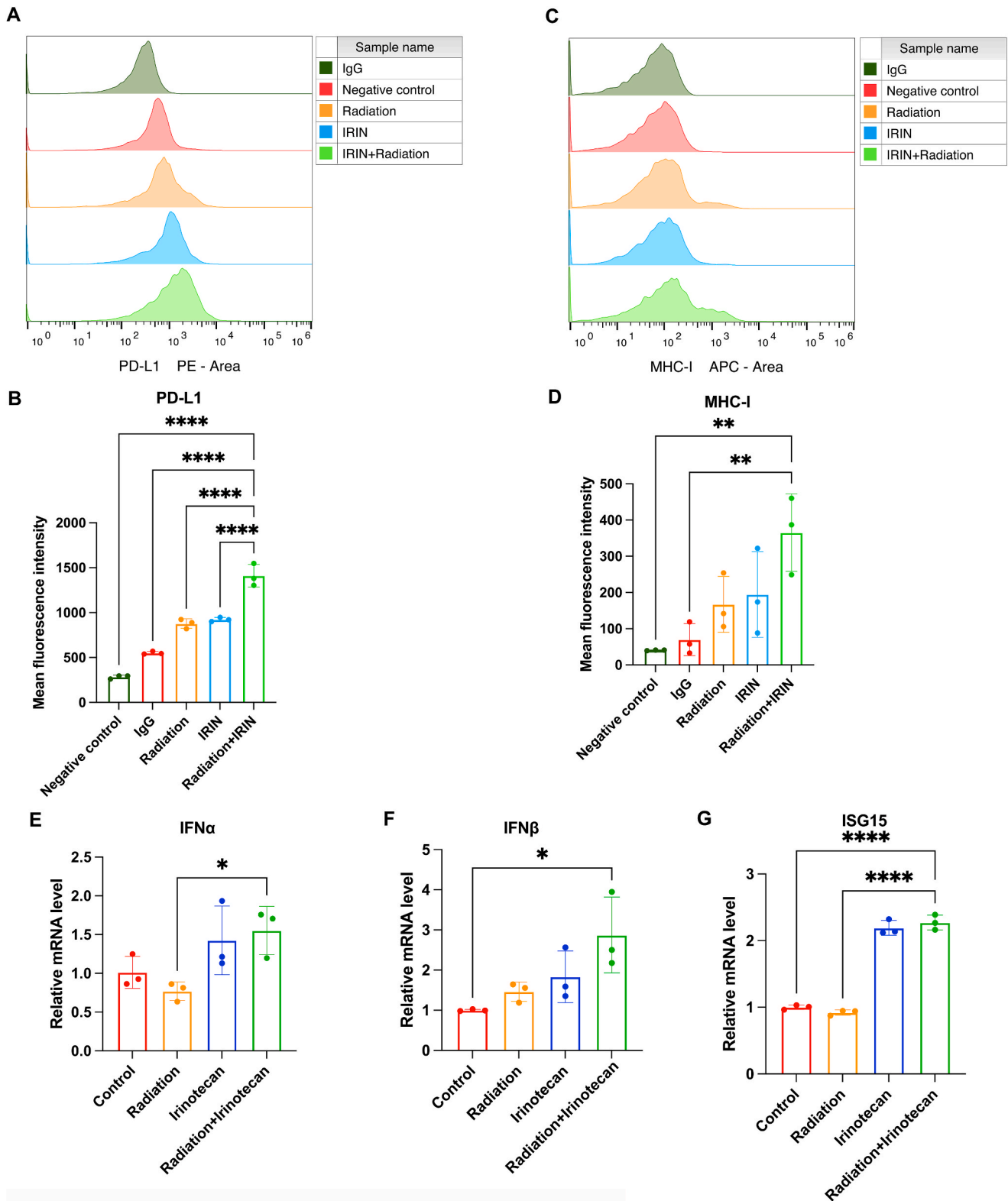
Fig. 3. IRIN plus radiation therapy significantly increased antigen presentation and PD-L1 expression level in CRC cells (A) (C) The expression levels of PD-L1 (A) and MHC-I (C) in HCT8 cells with different treatments were analyzed by flow cytometry. IgG group represented control cells that were stained with isotype IgG. Negative control group represented control cells that were stained with PD-L1 or MHC-I antibody. Radiation group represented cells irradiated with 4 Gy X-rays that were stained with PD-L1 or MHC-I antibody. IRIN group represented cells treated with 3 μM IRIN that were stained with PD-L1 or MHC-I antibody. IRIN plus radiation group represented cells treated with 3 μM IRIN and 4 Gy X-rays that were stained with PD-L1 or MHC-I antibody. (B) (D) Quantitation of fluorescent intensity of PD-L1 (B) and MHC-I (D). Data were presented as the mean $\pm$ SD obtained from three independent experiments. (E–G) qRT-PCR analysis of the expression level of IFN-α (E), IFN-β (F), ISG15 (G). (H–I) ELISA assays of IFN-α (H) and IFN-β (I) level in the supernatant. (J–K) qRT-PCR analysis of the expression level of NLRC5 (J) and TAP1 (K). Data were presented as the mean $\pm$ SD obtained from three independent experiments. (J) Representative Western blot images of β2M. Quantitation of β2M protein level was performed by ImageJ software. $*P < 0.05$, $**P < 0.01$, $***P < 0.001$, $****P < 0.0001$ (One-way ANOVA, followed by Tukey's test).
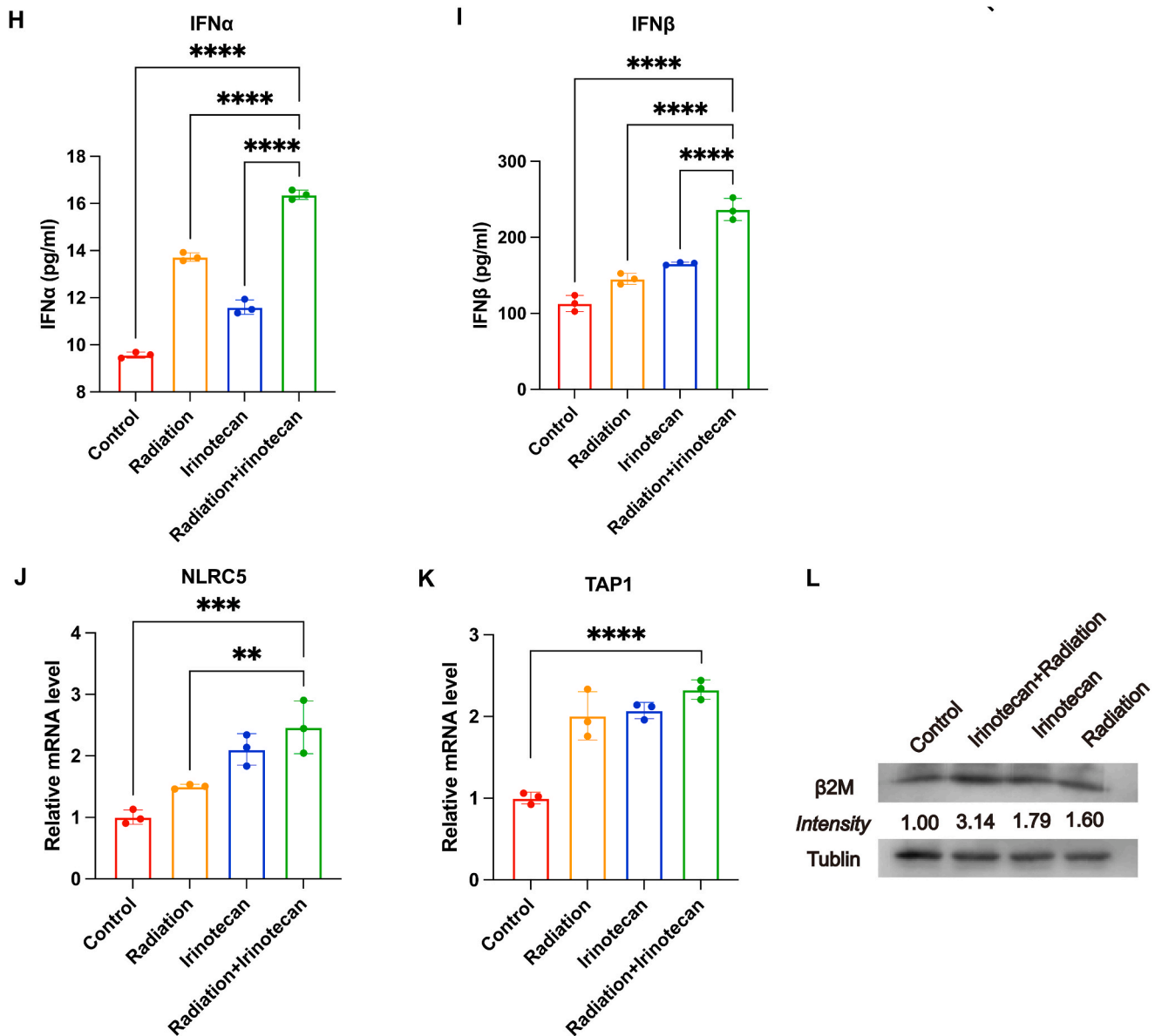
Fig. 3. (*continued*).

IRIN silicasome has the same biological effect as the free IRIN *in vitro*, CCK-8 assay was employed to detect the IC$_{50}$ of IRIN silicasome and free IRIN in CRC cells (Fig. 4C). IRIN silicasome concentrations were calculated using concentrations equivalent to IRIN. The results showed that the IC$_{50}$ curves for the two drugs were almost identical, indicating that they have equivalent efficacy in inhibiting tumor growth *in vitro*. Furthermore, the effects of free IRIN and IRIN silicasome on the activation of the cGAS/STING pathway were assessed in murine syngeneic CRC MC38 cells (Fig. 4D). Similar to the effects on human tumor cells, the results of western blotting revealed that free IRIN combined with radiation therapy significantly increased the protein expression levels of STING, *p*-IRF3, and *p*-TBK1 compared with the single treatment and control group. IRIN silicasome showed the similar potency to free IRIN, while empty silicasome had no effect on the activation of the cGAS/STING pathway.

2.5. In vivo potency of IRIN silicasome plus radiation therapy

To evaluate the potency and distribution of silicasome as a carrier for IRIN *in vivo*, experiments were conducted using immunocompetent C57BL/6 mice bearing luciferase MC38 tumors. Mice received a single intravenous (IV) injection of DyLight680-labeled silicasome whose dose was equivalent to 40 mg/kg IRIN. *Ex vivo* imaging using IVIS was performed to visualize the distribution of the silicasome in the tumors and organs of mice at 48 h after the injection (Fig. 5A). The quantitation of average near-infrared (NIR) fluorescence intensity for tumors and organs was also carried out (Fig. 5B). The results indicated that particles were mainly distributed in the primary tumor site, liver, kidney, and spleen. Confocal microscopy was performed to analyze the intratumoral distribution of the silicasome (Fig. 5C), which showed that the silicasome was distributed throughout the tumor and was present in a close proximity to the tumor blood vessels (stained with CD31). These results are consistent with the previously reported findings concerning distribution of silicasome in the pancreatic or CRC orthotopic models [26,46, 47]. To further confirm the advantages of using silicasome for IRIN delivery, the pharmacokinetics (PK) and tumor drug content of IRIN that delivered as free drug or by silicasome nanocarrier were assessed. As shown in the PK profile (Fig. 5D), the silicasome remarkably increased the drug circulation time and led to a significantly higher plasma area under the curve (AUC) value. The circulatory t$_{1/2}$ of IRIN silicasome was
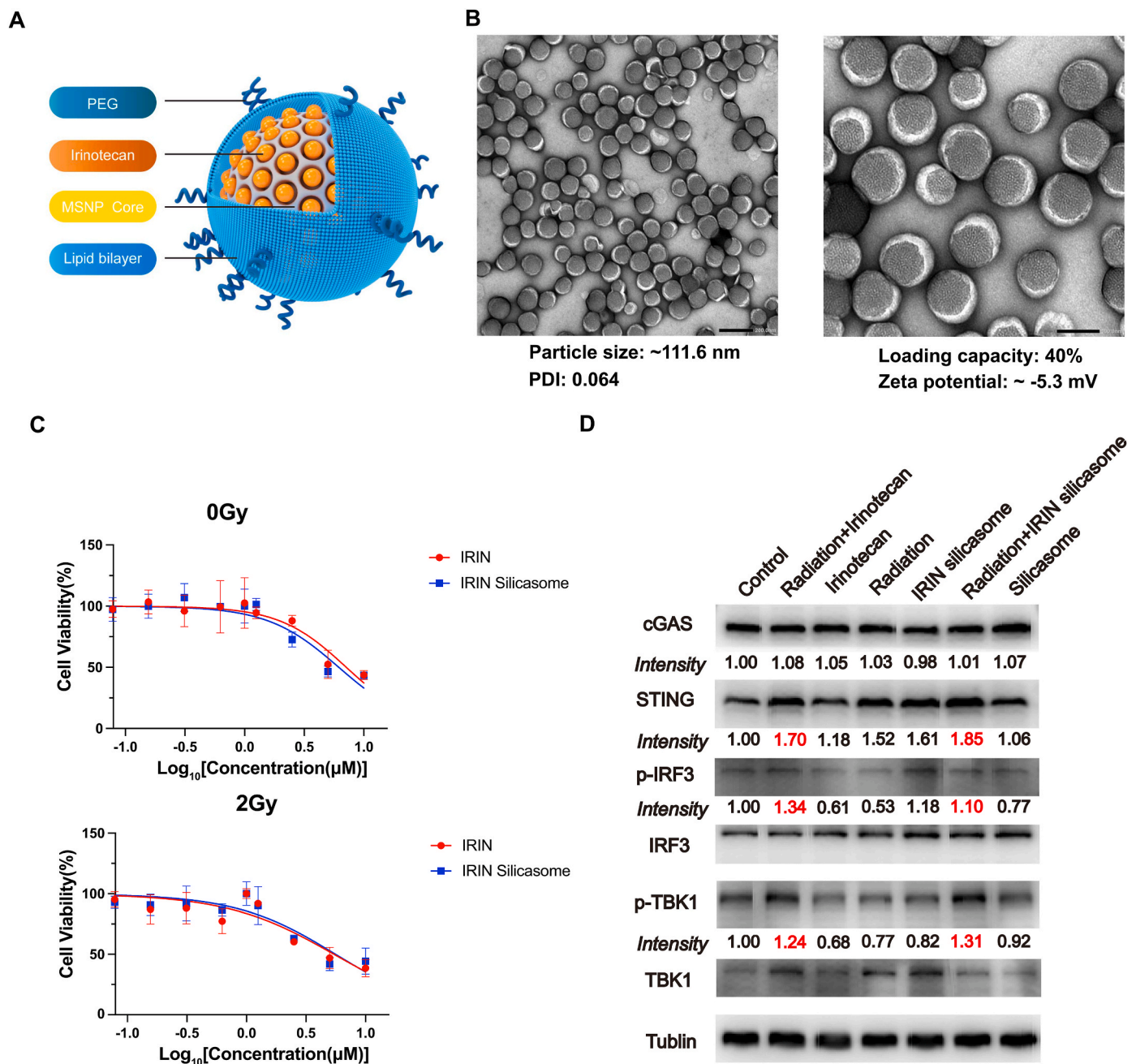
Fig. 4. Confirmation of the activation of the cGAS/STING pathway for radiation therapy plus IRIN when delivered by a silicasome nanocarrier (A)The scheme of IRIN silicasome nanocarrier. (B) Representative transmission electron microscopic images of IRIN silicasomes. The negative staining showed the uniform lipids coating on the MSNP. Bar: 200 nm (left); 100 nm (right). The particle morphology, hydrodynamic size, polydispersity index (PDI), zeta potential, and loading capacity were shown. (C) IC$_{50}$ curves. HCT8 cells were treated with different concentrations of free IRIN and IRIN silicasome for 48 h. The cell viability was assessed by CCK-8 assay. Each point represents the mean $\pm$ SD of three independent experiments. IC$_{50}$ was calculated with the nonlinear regression analysis by GraphPad Prism software. (D) Western blot analysis was conducted to measure the effects of free IRIN and IRIN silicasome on the activation of the cGAS/STING pathway in MC38 cells. ImageJ software was used to determine protein levels normalized to the tublin band.

12.34 $\pm$ 3.23 h. For free IRIN, t$_{1/2}$ alpha was 0.01 $\pm$ 0.01 h and t$_{1/2}$ beta was 9.18 $\pm$ 1.74 h. The plasma AUC values for IRIN silicasome and free drug were 1089.36 $\pm$ 131.18 and 13.96 $\pm$ 4.00 μg/ml*h, respectively. The IRIN content in the tumor was measured at 48 and 72 h after a single IV injection of the drug at the same dose as free drug or loaded in silicasome. The 48-h IRIN content for free IRIN and IRIN silicasome was 0.012 $\pm$ 0.001 and 9.545 $\pm$ 5.103 μg/g tumor, respectively. Besides, the 72-h IRIN content for free IRIN and IRIN silicasome was 0.011 $\pm$ 0.003 and 2.957 $\pm$ 0.315 μg/g tumor, respectively. The results demonstrated that the IRIN content in the tumor was significantly higher when it was

delivered by silicasome compared with the free drug (Fig. 5E). It was also attempted to compare silicasome with the commercial IRIN liposome. The drug content in tumor delivered by silicasome was also significantly higher than that of liposome in the MC38 subcutaneous model (Fig. S2A). The IRIN content of liposome for 48 and 72 h was 0.328 $\pm$ 0.128 and 0.178 $\pm$ 0.076 μg/g tumor, respectively.

According to the improved drug delivery profile using silicasome, the antitumor efficacy of radiation therapy combined with IRIN delivered as free drug or by silicaosme was assessed (Fig. 5F). The MC38 tumor-bearing mice were treated with free IRIN and IRIN silicasome at an
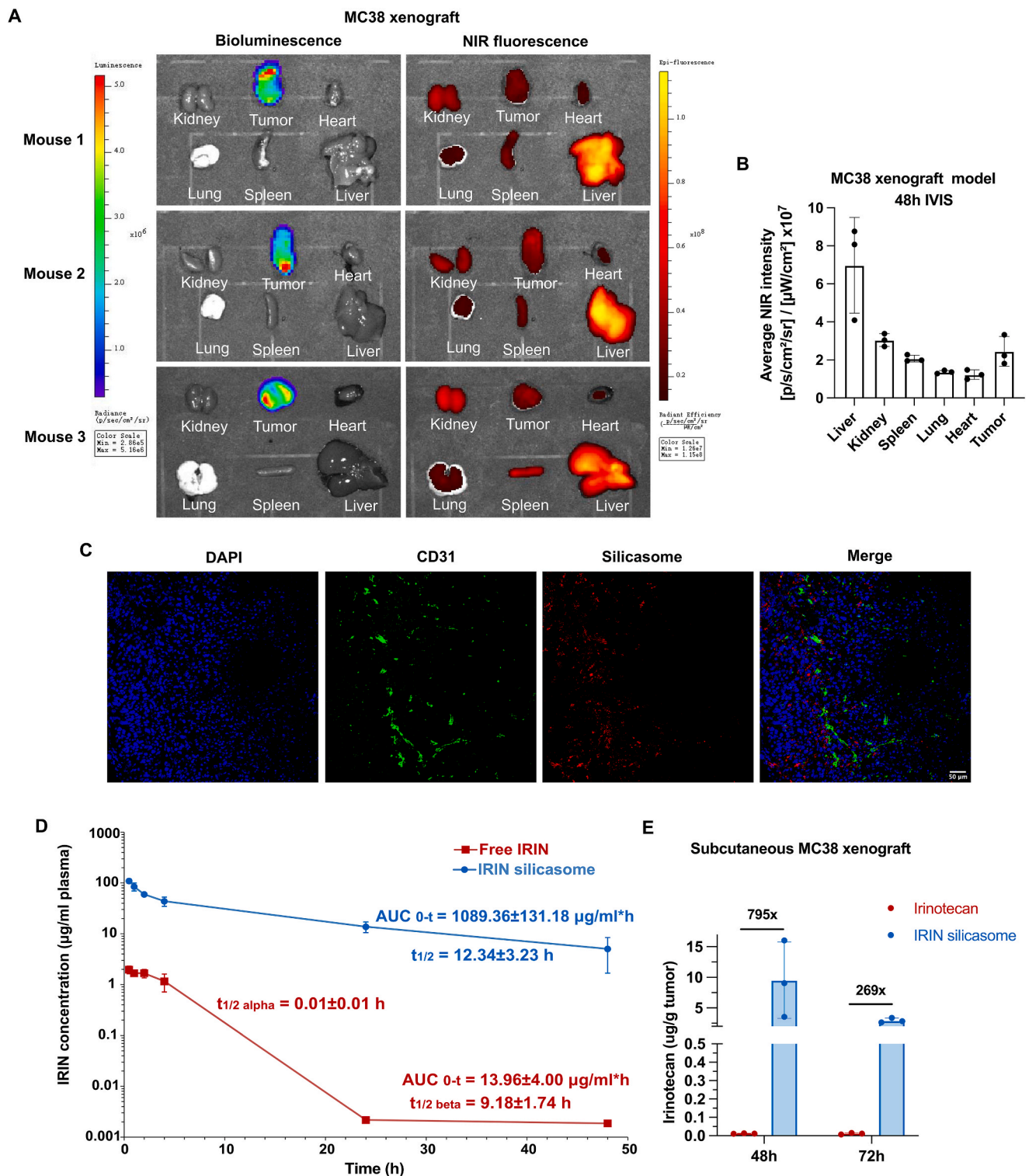
Fig. 5. The effects of IRIN silicasome plus radiation therapy on the CRC xenograft tumor model (A) *Ex vivo* IVIS imaging of mice with subcutaneous tumor receiving IV injection of DyLight680-labeled silicasome. Tumor and organs were harvested at 48 h after a single IV injection of silicasome at an IRIN equivalent dose of 40 mg/kg. (B) Quantitation of average NIR fluorescence intensity for tumors and organs. Mice that did not receive silicasome served as background tissue autofluorescence. Data were presented as mean ± SD (n = 3). (C) Confocal laser scanning microscopy of silicasome distribution in murine tumor used in (A). Red: DyLight680-labeled silicasome. Green: Blood vessels stained with CD31. Blue: DAPI. Scale bar: 50 μm. (D) PK profile of a single IV injection of free IRIN or IRIN silicasome at an IRIN equivalent dose of 40 mg/kg (n = 3). Circulatory $t_{1/2}$ and AUC_{0-t} values were calculated using PKSolver software. (E) IRIN content in the tumor at 48 and 72 h after a single IV injection of 40 mg/kg IRIN by the different carriers (free drug and silicasome). (F) Tumor volume measurement of MC38 subcutaneous xenograft tumor in different treatment groups (n = 6). Mice were treated with free IRIN and IRIN silicasome at an IRIN equivalent dose of 40 mg/kg IV every 3 days with a total of four administrations (red arrow). Radiation therapy was performed on the day after chemotherapy with an X-ray irradiator (SARRP3) (blue arrow). The dose was 2 Gy X-rays per fraction with a total of 4 fractions. Treatment was initiated when the tumor volume reached ~100 mm³. Data were analyzed by ANOVA, followed by Tukey's test. *$P < 0.05$, **$P < 0.01$, ***$P < 0.001$, ****$P < 0.0001$. (For interpretation of the references to colour in this figure legend, the reader is referred to the Web version of this article.)
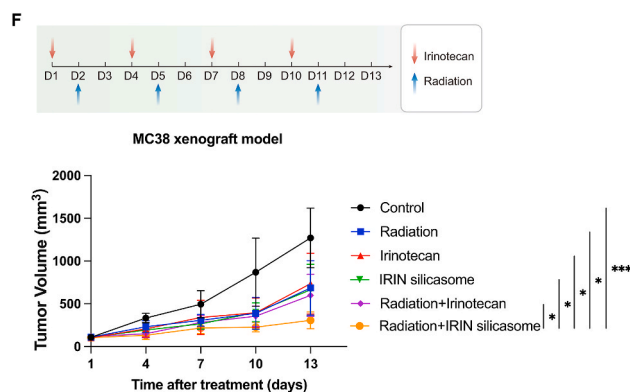
Fig. 5. (*continued*).

equivalent dose of 40 mg/kg IV every 3 days, totally including four administrations. Mice were also subjected to radiation therapy with an X-ray irradiator on the day after chemotherapy. The radiation dose was 2 Gy per fraction with a total of 4 fractions. The treatment was initiated when the tumor volume reached ~100 mm^3. It was revealed that mice treated with the combination of IRIN silicasome and radiation therapy had the smallest tumor volume, demonstrating the superior efficacy of radiation therapy combined with silicasome as a carrier for IRIN in comparison with the free drug. In addition, IRIN liposome combined with radiation therapy also showed a superior efficacy to that of the IRIN liposome group and control group, while it was less effective than the silicasome combination (Fig. S2B). The HE staining of the heart, liver, spleen, lung, and kidney showed that there was no obvious organ toxicity in the combined treatment group compared with the control group (Fig. S3).

2.6. IRIN silicasome plus radiation therapy activated TIME that led to a robust efficacy after combination with anti-PD-1

Several studies have reported a close relationship between the activation of the cGAS/STING pathway and tumor immunity [48,49]. Therefore, the effect of IRIN silicasome plus radiation therapy on the TIME were explored in the present study. The flow cytometry was employed to examine the proportion of immune cells in tumors after different treatments, including control group, radiation group (2 Gy X-rays for 4 fractions, every 3 days), IRIN silicasome group (40 mg/kg for 4 administrations, every 3 days), and combined treatment group of IRIN silicasome and radiation therapy (2 Gy X-rays for 4 fractions, 40 mg/kg IRIN for 4 administrations, IRIN was given on the day before radiation therapy) as the same experiment illustrated in Fig. 5E. Animals were sacrificed at 48 h after the last radiation therapy, and tumor tissues were digested for single-cell flow cytometry analysis of the proportion of CD4$^+$ and CD8$^+$ T cells and CD11c$^+$ DC cells (gating strategies were provided in Fig. S4 amd S5). The results showed an increase in the proportion of CD4$^+$ and CD8$^+$ T cells (Fig. 6A, C, 6D) and CD11c$^+$ DC cells (Fig. 6B and E) in tumors treated with IRIN silicasome plus radiation therapy compared with those treated with IRIN silicasome or radiation therapy alone. Immunofluorescence staining also confirmed the increase in the number of CD4$^+$ and CD8$^+$ T cells and IFN-γ expression level (Fig. 6F–I) in tumors treated with IRIN silicasome plus radiation therapy. These findings demonstrated that the combination of IRIN silicasome with radiation therapy could activate the immune microenvironment in mice bearing tumors. It was suggested that the combination of IRIN silicasome with radiation therapy may be a potential treatment strategy for activating the immune response in tumors, thereby enhancing the efficacy of immunotherapy.

According to the abovementioned findings, it was attempted to further investigate the potential of *anti*-PD-1 treatment in combination with IRIN silicasome plus radiation therapy (Fig. 6J). Mice were treated

with IRIN silicasome at an equivalent dose of 40 mg/kg IV every three days, totally including four administrations. On the day after chemotherapy, mice were irradiated with 2 Gy X-rays for four fractions. Then, 100 µg *anti*-PD-1 antibody was intraperitoneally (IP) injected on the day after radiation therapy for three administrations. The results revealed that addition of *anti*-PD-1 treatment further improved the effectiveness of the combination therapy, leading to achieve more promising outcomes in terms of tumor regression.

3. Discussion

In the present study, the synergistic effects of IRIN plus radiation therapy were assessed via the increased DNA damage and the ability of activating the cGAS/STING pathway. It was revealed that the combination of IRIN chemotherapy with radiation therapy could not only result in a greater antitumor efficacy, but also activate the TIME in CRC. It was found that IRIN combined with radiation therapy significantly increased the generation of intracellular ROS and enhanced the level of apoptosis. As radiation therapy and numerous chemotherapeutic drugs kill tumor cells by damaging their DNA [30], the present study indicated that DNA damage was dramatically risen in the combined treatment group. It could be speculated that the synergistic mechanism of the two could be achieved by increasing DNA damage. DNA damage can lead to the accumulation of dsDNA in the cytoplasm. The present study indicated that the content of dsDNA in the combined treatment group was more than that in the single treatment group and the control group. Further experiments revealed that the cGAS/STING-dependent type I IFN pathway was also activated. It was also found that antigen presentation and PD-L1 expression level in tumor cells were elevated in the combined treatment group. This provides a basis for *in vivo* activation of the TIME and immunotherapy. Furthermore, it was revealed that IRIN delivered by a silicasome nanocarrier could activate the cGAS/STING pathway when combined with radiation therapy. *In vivo* experiments indicated that IRIN silicasomes plus radiation therapy had the strongest tumor regression effect compared with other individual treatments or free drug combination. Furthermore, the combination therapy significantly increased the proportion of CD4$^+$ and CD8$^+$ T cells in the tumor microenvironment, accompanying by the increased IFN-γ production, which indicated the activated function of T cells. The proportion of CD11c$^+$ DC cells was also risen in the combined treatment group. The *anti*-PD-1 therapy was combined with IRIN silicasome plus radiation therapy. The results suggested that the combination of the three treatment modalities further improved antitumor efficacy.

The National Comprehensive Cancer Network (NCCN) guidelines recommended that for patients with locally advanced rectal cancer, the standard treatment is preoperative fluorouracil-based nCRT, followed by TME surgery. Patients who responded to nCRT and achieved pCR had a better prognosis than those who did not respond. If the patient achieves cCR after nCRT, a watch-and-wait strategy can be adopted to
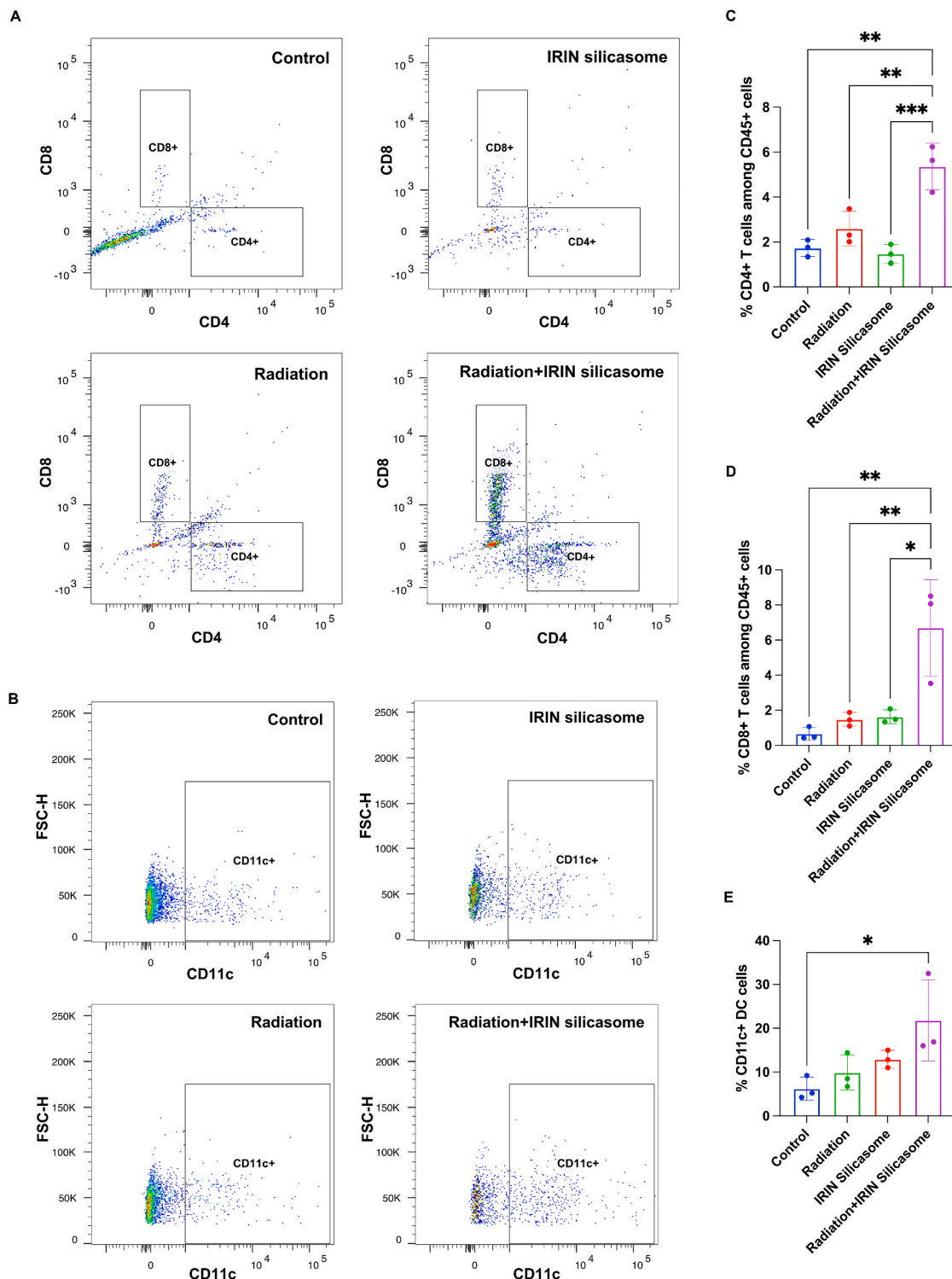
Fig. 6. IRIN silicasome plus radiation therapy activated TIME that led to a robust efficacy via further combination with *anti*-PD-1 (A) Flow cytometry of CD4$^+$ and CD8$^+$ T cells in tumors received different treatments. Dot plots show the proportion of CD4$^+$ and CD8$^+$ T cells. (B) Flow cytometry of CD11c$^+$ DC cells in different groups. (*C*–D) Quantitation of the percentage of CD4$^+$ T cells (C) and CD8$^+$ T cells (D) among CD45$^+$ T cells (n = 3). (E) Quantitation of the percentage of CD11c$^+$ DC cells among non-macrophages (n = 3). (F) Multicolor immunofluorescence staining of tumors with different treatments. Green: CD4. Red: CD8. Yellow: IFN-γ. Blue: DAPI. Scale bar: 50 μm. (G–I) Quantitation of the amount of CD4 (G), CD8 (H), and IFN-γ (I) protein expression levels in integrated option density (IOD) by ImageJ software. Each group consisted of three mice. (J) Tumor volume of MC38 subcutaneous xenograft tumor in different treatment groups (n = 6). Mice were treated with IRIN silicasome at an IRIN equivalent dose of 40 mg/kg IV every 3 days with a total of four administrations (red arrow). Radiation therapy was performed on the day after chemotherapy (blue arrow). The dose was 2 Gy per fraction with a total of 4 fractions. 100 μg *anti*-PD-1 antibody was injected IP on the day after radiation therapy for a total of 3 administrations (green arrow). Data were analyzed by ANOVA, followed by Tukey's test. *P < 0.05, **P < 0.01, ***P < 0.001, ****P < 0.0001. (For interpretation of the references to colour in this figure legend, the reader is referred to the Web version of this article.)
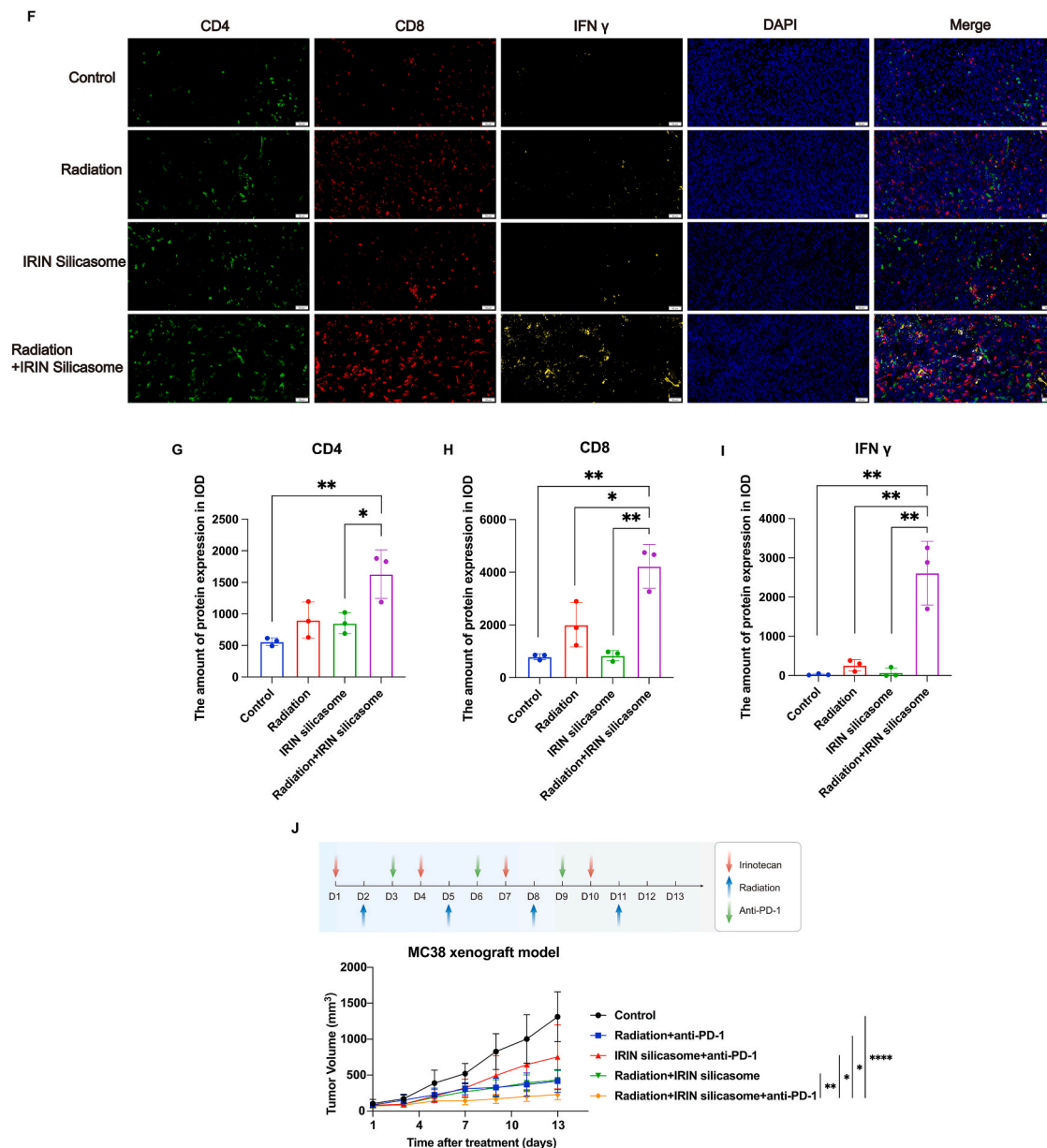
Fig. 6. (*continued*).

achieve the purpose of preserving organ function and improving the patient's quality of life [2]. However, only 10–15% of patients can currently achieve pCR [4]. Therefore, how to improve the efficacy of nCRT is vital clinically. To this end, our team previously conducted a clinical trial to optimize nCRT for this issue [16]. IRIN is an effective chemotherapeutic drug with severe side effects in CRC. Due to its toxicity, it is difficult for IRIN to achieve an effective therapeutic dose. IRIN was added to nCRT, and the dosage was individually adjusted according to the genotype of UGT1A1. The results revealed that the pCR rate was elevated to 30%. However, the incidence of IRIN-related adverse effects, such as diarrhea and neutropenia, significantly increased. Therefore, it is suggested to optimize the administration of IRIN, so as to promote the combined application of IRIN and radiotherapy.

Although IRIN liposome was approved for the treatment of advanced pancreatic cancer [50], a phase II clinical trial of Onivyde monotherapy in CRC exhibited disappointing results [51], leading to a temporary abandonment of exploration in CRC. In addition, the FDA has warned about "severe neutropenia and severe diarrhea" for IRIN liposomes [50].

However, with the development of our designed IRIN silicasome, it is feasible to reconsider IRIN nanoformulation for the treatment of CRC. It is suggested to replace IRIN with IRIN silicasome in nCRT and indicate whether the dose of IRIN can be increased within the acceptable adverse effect range to achieve a greater tumor control. Currently, numerous scenarios exist where silicasomes find applications in various translation. Regarding nano immunotherapy research, silicasomes were incorporated with a GSK3 inhibitor (AZD1080), which acted on the PD-1/PD-L1 axis. As a result of this combination, notable T cell activation was induced in models of pancreatic cancer and CRC, leading to notable anti-tumor effects [52]. The CDK4/6 inhibitor, palbociclib, and the autophagy inhibitor, hydroxychloroquine, were co-encapsulated in silicasomes. This combination exhibited synergistic effects in subcutaneous and orthotopic mouse models of pancreatic cancer [53]. Moreover, the challenge of scaling up silicasome synthesis has also been overcome [26], which demonstrated promising translation development based on the manufacture, efficacy and safety considerations [54,55]. In the present study, no significant difference was found in tumor inhibition between the single treatment of free IRIN drug alone and IRIN

silicasome in the subcutaneous MC38 xenograft, which is different from our previous findings in the more aggressive orthotopic xenograft [26]. However, after their combination with radiation therapy, the efficacy of the IRIN silicasome group was superior to the free IRIN drug group in the subcutaneous model. It indicated that the *in vivo* synergic effect with radiation therapy requires a higher effective tumor drug concentration, which is consistent with our clinical results that patients benefited more from the combination therapy when the dose of IRIN was elevated based on UGT1A1 expression level [16]. Moreover, the radiation therapy could promote the delivery of nanomedicines in tumors by increasing the vascular permeability [56,57], which could further benefit the combination of radiation therapy with silicasome nanocarrier.

Another important finding of this study is that IRIN combined with radiation therapy could significantly activate the cGAS/STING pathway. Moreover, IRIN silicasome plus radiation therapy could activate the TIME *in vivo*. To date, several studies have shown that topoisomerase (Top) inhibitors may activate the cellular endogenous immune pathway cGAS/STING. Pépin et al. demonstrated that Top II inhibitors could induce the activation of the IFN-I pathway through the ATM and cGAS/STING pathways, thereby preventing Ebola virus infection [58]. Top I inhibitors may activate the cGAS/STING pathway through induced micronuclei, whereas loss of cGAS or STING may avert activation of IFN-related pathways [59]. In addition, Top I inhibitors may induce cytoplasmic DNA leakage by inducing nuclear DNA damage, thereby activating the cGAS/STING pathway [58]. Similarly, radiation therapy activates the cGAS/STING pathway in tumor cells by inducing DNA damage. Tumor cells release inflammatory factors to recruit immune cells to alter the tumor microenvironment. In addition, the body's immunity is activated and the unirradiated tumor at the remote site regresses, which is called the abscopal effect, and the absence of STING may weaken abscopal effect [60,61]. Besides, radiation-induced vascular hyperpermeability may allow the recruitment of more immune cells in the tumor microenvironment [62]. Consistently, in the present study, IRIN silicasome and radiation therapy produced a synergistic effect, significantly activating the cGAS/STING pathway. *In vivo* experiments revealed that the combination of the two remarkably increased the number of CD4$^+$ and CD8$^+$ T cells in the tumor microenvironment and activated the function of T cells. The number of DCs was also elevated. This provides a solid basis for further combination with checkpoint inhibitor inhibitors.

In summary, the results of the present study demonstrated that IRIN combined with radiation therapy had a significant synergistic killing effect and could induce cGAS/STING-mediated activation of type I IFN in CRC cells. The application of IRIN silicasome nanocarrier plus radiation therapy could remarkably activate the immune microenvironment, thereby making tumors more sensitive to *anti*-PD-1 therapy. Some clinical trials of IRIN combined with radiotherapy in the treatment of locally advanced rectal cancer are in progress. In this study, more efficient delivery of IRIN through silicasome is expected to further activate the TIME on the basis of improving efficacy. It provides a strong basis for the clinical optimization of nCRT for rectal cancer.

4. Methods

4.1. Cell culture

Human CRC cell lines (HCT8 and HT29) and murine CRC cell line MC38 were purchased from the American Type Culture Collection (ATCC; Manassas, VA, USA). Cells were cultured in a Dulbecco's modified Eagle's medium (DMEM; KeyGEN BioTECH Co., Ltd., Nanjing, China) supplemented with 10% fetal bovine serum (Sigma-Aldrich, St. Louis, MO, USA) and 100 U/ml penicillin and 100 μg/ml streptomycin (KeyGEN BioTECH Co., Ltd.) in a humid atmosphere of 5% CO_2 and 95% air.

4.2. Cell viability assay

Cells were seeded into 96-well plates with a density of 5000 cells per well. After the cells were adhered to the wall, different concentrations of IRIN (Hengrui Pharmaceuticals Co., Ltd., Jiangsu, China) free drug and IRIN silicasome were added. After 12 h of drug treatment, they were exposed to different doses of radiation therapy. After 48 h of irradiation, CCK-8 solution (Targetmol) was added according to the manufacturer's instructions, and the absorbance value was detected at a wavelength of 450 nm using a microplate reader.

4.3. Colony formation assay

Cells (150–1200/well) were seeded into 6-well plates and irradiated with different doses (0, 2, 4, 6 Gy). After irradiation, cells were cultured for 14 days to form colonies, then, they were fixed with 4% para-formaldehyde and stained with crystal violet. Colonies (>50 cells) were counted to calculate survival fraction, and survival curves were fitted to a model (SF = 1-(1-exp (−k*D))^N) based on a single-hit multi-targeted model. In the IRIN group, cells were pretreated with 1 μM IRIN for 12 h before irradiation, and the medium was changed to remove the drug before irradiation.

4.4. ROS detection

The level of intracellular ROS was detected using the ROS assay kit (Beyotime Institute of Biotechnology, Nanjing, China) according to the manufacturer's protocol. Cells were seeded into 6-well plates at the density of 5×10^5 cells per well, and different treatments were performed after the adherence of cells to the wall. In the radiation group, the irradiation dose was 4 Gy. In the IRIN group, the drug concentration was 3 μM. In the IRIN combined with radiation group, 3 μM IRIN was added at 12 h before irradiation, followed by 4 Gy irradiation. After 2 h of irradiation, 2,7-dichlorodi-hydrofluorescein diacetate (DCFH-DA) was added to the cells and incubated at 37 °C for half an hour, followed by imaging under a fluorescence microscope.

4.5. Apoptosis assay

An Annexin V-APC/PI apoptosis kit (MULTISCIENCES Biotech Co., Ltd., Hangzhou, China) was used to detect the rate of apoptosis. Cells were seeded into 6-well plates at the density of 5×10^5 cells per well, and different treatments were performed after the adherence of cells to the wall. In the radiation group, the irradiation dose was 4 Gy. In the IRIN group, the drug concentration was 3 μM. In the IRIN combined with radiation group, 3 μM IRIN was added at 12 h before irradiation, followed by 4 Gy irradiation. After 48 h of irradiation, the cells were digested with trypsin to form a single-cell suspension, then, they were resuspended in 500 μl binding buffer, incubated with 5 μl Annexin V and 10 μl PI for 10 min at room temperature, and they were finally analyzed by a flow cytometer (Sony Biotechnology Inc., Tokyo, Japan).

4.6. Immunofluorescence assay

Detection of γ-H2AX and dsDNA: The cell culture medium was discarded, and the cells were twice washed with phosphate-buffered saline (PBS). After adding 4% paraformaldehyde solution to fix the cells for 10 min, the cells were permeabilized by 0.2% Trion X-100 for 10 min, and blocked with 3% bovine serum albumin (BSA) for 30 min. Cells were incubated overnight at 4 °C with primary antibodies at a dilution ratio of 1:200, including γ-H2AX (#9718 S; Cell Signaling Technology, Danvers, MA, USA) and dsDNA (#ab27156; Abcam, Cambridge, UK) antibodies. After twice washing with PBS, the cells were incubated with 1:500 diluted fluorescent secondary antibody (#A0428; # A0423; Beyotime Institute of Biotechnology) for 60 min. Cells were washed with PBS and sealed with 4′,6-diamidino-2-phenylindole (DAPI)-containing anti-

fluorescence quenching sealing tablets (Beyotime Institute of Biotechnology). Cells were observed and photographed by a confocal laser scanning microscope (A1 HD25; NIKON, Tokyo, Japan).

4.7. Western blotting

The total protein of the cells was extracted with RIPA lysis buffer (Beyotime Institute of Biotechnology). After measuring protein concentration by a BCA protein assay kit (Beyotime Institute of Biotechnology), 30 μg of protein was loaded and separated by 10% sodium dodecyl-sulfate polyacrylamide gel electrophoresis (SDS-PAGE) gel, transferred onto polyvinylidene difluoride (PVDF) membrane (Millipore, Boston, MA, USA), blocked with 5% BSA diluted with 0.05% Tris-buffered saline/Tween (TBST) for 2 h, and incubated with the primary antibody overnight at 4 °C. The antibody information is listed in Table S1. Then, it was incubated with horseradish peroxidase-conjugated IgG secondary antibody (Beyotime Institute of Biotechnology) for 2 h at room temperature. Protein bands were exposed using an enhanced chemiluminescence kit (Millipore).

4.8. Flow cytometric analysis of MHC-I and PD-L1

Cells were digested into a single-cell suspension using PBS containing 0.2% EDTA. Cells were centrifuged at 200 g for 3 min and twice washed with PBS. Cells were resuspended in 500 μl binding buffer, and stained with MHC-I (APC anti-human HLA-A, B, C; #311410; Bio-Legend, San Diego, CA, USA) and PD-L1 (PE anti-human CD274; 329,707; Biolegend) antibodies for 30 min on ice. The IgG group was incubated with an equal amount of isotype IgG (#400219; #400313; BioLegend). Cells were twice washed with PBS and were then detected by flow cytometry.

4.9. Reverse transcription polymerase chain reaction (qRT-PCR)

An RNA extraction kit (Sparkjade Scientific Instruments Co., Ltd., Shandong, China) was used to isolate RNA from cells. Reverse transcription of total RNA to cDNA was performed in 20 μl reaction reagents of a reverse transcription kit (Sparkjade Scientific Instruments Co., Ltd.) according to the manufacturer's protocol. The qRT-PCR was performed using the SYBR Green qPCR kit (Sparkjade Scientific Instruments Co., Ltd.). Primers used for qRT-PCR are listed in Supplementary Table S2. In the radiation group, the irradiation dose was 4 Gy. In the IRIN group, the cells were treated with 3 μM IRIN for 36 h. In the IRIN plus radiation group, cells received 4 Gy X-rays after 12 h of IRIN pretreatment.

4.10. ELISA

ELISA assays were performed with human IFN-α ELISA kit (MULTI-SCIENCES Biotech Co., Ltd., Hangzhou, China) and human IFN-β ELISA kit (NEOBIOSCIENCE Biotech Co., Ltd., Shenzhen, China). The radiation group was irradiated with 4 Gy X-rays. The IRIN group was treated with 3 μM IRIN. The combination group was treated with 4 Gy X-rays and 3 μM IRIN. After 48 h, the supernatant of cell was extracted and centrifuged at 300 g for 10 min, which was used for ELISA tests.

4.11. Synthesis and characterization of IRIN silicasomes

The IRIN silicasomes were prepared as previously described [46]. After bare MSNPs were synthesized, acidic ethanol was used to remove cetyltrimethylammonium chloride (CTAC) to purify mesoporous silica nanoparticles (MSNPs). Trapping agent triethylamine sucrose octasulfate (TEA$_8$SOS) solution was prepared using sucrose sodium octasulfate. After the lipid material (DSPC/cholesterol/DSPE-PEG2000 M ratio was 3: 2: 0.15) was dissolved in pure ethanol, it was added to the TEA$_8$SOS solution containing MSNPs, followed by probe sonication. TEA$_8$SOS was then removed using size exclusion chromatography.

Thereafter, the silicasome solution was mixed with the IRIN drug solution according to the silicasome/drug mass ratio of 2:1, and incubated at 65 °C for 1 h. The IRIN silicasomes were purified and sterilized by passing through a 220 nm filter.

Characterization of IRIN silicasomes was performed as previously described [46]. A particle and molecular charge analyzer (Zetasizer Nano ZS ZEN3600) was used to analyze the particle hydrodynamic size, polydispersity index (PDI), and zeta potential of silicasomes. The silicasomes were photographed using a transmission electron microscope (JEM-2100plus). A microplate reader was used to measure the absorption values of a series of concentrations of IRIN drug solutions to draw a standard curve. Then, the absorption value of the silicasome was measured and substituted into the standard curve to obtain the drug concentration in the silicasome. Loading capacity was calculated as the weight ratio of IRIN to MSNPs.

4.12. In vivo distribution of silicasomes

The experiment was conducted using mice bearing luciferase-transfected MC38 tumors. Mice received a single intravenous (IV) injection of DyLight680-labeled silicasome whose dose was equivalent to 40 mg/kg IRIN. After 48 and 72 h of the injection, ex vivo imaging was carried out using IVIS (IVIS Lumina Series III; PerkinElmer, Inc., Waltham, MA, USA) to visualize the distribution of the silicasome in the tumor and organs of mice. In addition, tumor tissues were embedded in optimal cutting temperature (OCT) compound and sectioned by a cryostat microtome. After fixation, the cells were permeabilized with 0.2% Trion X-100 for 10 min, washed with PBS, blocked with 3% BSA for 30 min, and incubated overnight at 4 °C with primary CD31 (#ab222783; Abcam) antibody prepared at a dilution ratio of 1:200. After the cells were twice washed with PBS, a 1:500 diluted fluorescent secondary antibody was added and incubated for 60 min. Finally, the cells were washed with PBS and sealed with DAPI-containing anti-fluorescence quenching sealing tablets (Beyotime Institute of Biotechnology). Sections were imaged with a confocal laser scanning microscope (A1 HD25; NIKON).

4.13. Measurement of plasma and tumor IRIN concentrations

Healthy female C57BL/6 mice (age, 10–12 weeks old) received a single IV injection of free IRIN or IRIN silicasome at a dose of 40 mg/kg IRIN. Blood samples were collected at 0.5, 1, 2, 4, 24, and 48 h. After serum extraction, IRIN was extracted using acidic methanol solution. Drug concentrations were subsequently detected using liquid chromatography–mass spectrometry (LC-MS; 6495C; Agilent Technologies Inc., San Diego, CA, USA). PK data of free IRIN and IRIN silicasome were analyzed by PKSolver software using a two-compartment model and a one-compartment model, respectively [63].

Drug content was determined in tumor tissue obtained from a MC38 xenograft tumor model. Tumor-bearing mice received a dose of 40 mg/kg IRIN by tail vein injection of free IRIN, IRIN liposome or IRIN silicasome. Animals were sacrificed after 48 and 72 h to collect tumor tissues. Tumors were weighed and homogenized in acidic methanol to measure drug concentrations by LC-MS.

4.14. Irradiation of cells and tumors

Cells and mice were irradiated with an X-ray irradiator (SARRP3; Xstrahl). For in vivo tumor irradiation, mice were anesthetized with sodium pentobarbital (75 mg/kg) and placed in the machine for the cone beam computed tomography (CBCT) scan. Then, the treatment plan was formulated according to the CBCT images, and the local irradiation of tumors was completed.

4.15. Evaluating the in vivo efficacy of IRIN silicasomes combined with radiation therapy and anti-PD-1 antibody using a CRC xenograft tumor model

Each C57BL/6 female mouse was subcutaneously injected with 5×10^5 luciferase-transfected MC38 cells, and the treatment was started when the tumor volume reached 100 mm^3. Mice were treated with free IRIN, IRIN liposome (Hengrui Pharmaceuticals Co., Ltd., Jiangsu, China), and IRIN silicasome at an equivalent dose of 40 mg/kg IV every 3 days, totally including four administrations. Mice were also subjected to radiation therapy with SARRP3 on the day after chemotherapy. The radiation dose was 2 Gy per fraction, totally including 4 fractions. The dose of *anti*-PD-1 antibody (Hengrui Pharmaceuticals Co., Ltd.) was 100 μg, which was injected intraperitoneally on the day after radiation therapy, and was totally administered for 3 times. Tumor size was measured every 2 or 3 days. The tumor size was calculated as follows: tumor size (mm^3) $=$ length $\times$ width^2 $\times$ 0.52. Mice were sacrificed at 48 h after the last treatment. Tumors were digested into single-cell suspensions, and cells were labeled with monoclonal antibodies against surface markers in FACS buffer (PBS containing 2% fetal bovine serum (FBS) and 1 mM EDTA). Sample data were acquired on BD LSRFortessa (BD Biosciences, San Diego, CA, USA) and analyzed using FlowJo software (TreeStar). Antibody information is listed in Supplementary Table S3. Another murine tumor was used for multicolor immunofluorescence staining. The tumor was fixed in 10% formalin, and it was then paraffin-embedded and sectioned. Multicolor immunofluorescent staining was performed using the automated multiplex immunohistochemistry stainer (BOND RXm; Leica, Wetzlar, Germany). Slides were scanned using a slide scanner (VS200; Olympus, Tokyo, Japan) and images were evaluated. Antibody information is listed in Supplementary Table S4. The heart, liver, spleen, lung, and kidney of mice were fixed, embedded and sectioned, and were then stained with HE.

4.16. Statistics

Data were analyzed by ANOVA, followed by Tukey's test. $P < 0.05$ was considered significant.

4.17. Study approval

All animal experiments were performed in accordance with the ethical protocol approved by the Animal Research Committee of the Hangzhou Institute of Medicine (HIM), Chinese Academy of Sciences (Hangzhou, China).

Credit author statement

Lu Wang: Writing – original draft, Data curation, Formal analysis, Investigation, Visualization. Tianyu Zhang: Data curation, Formal analysis, Investigation, Methodology. Yile Zheng: Methodology, Visualization. Yuting Li: Methodology, Visualization. Xiyuan Tang: Data curation, Validation. Qianping Chen: Methodology, Validation. Wei Mao: Methodology, Validation. Weiwei Li: Investigation, Methodology. Xiangsheng Liu: Conceptualization, Funding acquisition, Resources, Supervision, Writing – review & editing. Ji Zhu: Conceptualization, Funding acquisition, Resources, Supervision, Project administration, Writing – review & editing.

Declaration of competing interest

The authors declare that they have no known competing financial interests or personal relationships that could have appeared to influence the work reported in this paper.

Data availability

Data will be made available on request.

Appendix A. Supplementary data

Supplementary data to this article can be found online at https://doi.org/10.1016/j.mtbio.2023.100809.

References

[1] American Cancer Society, Estimated Deaths (2023). https://cancerstatisticscenter.cancer.org/module/yg6E0ZLc. (Accessed 13 February 2023).

[2] National Comprehensive Cancer Networks (NCCN), The NCCN rectal cancer clinical practice guidelines in oncology (version 5 2023) [EB/OL] (2023).

[3] M.J.M. van der Valk, D.E. Hilling, E. Bastiaannet, et al., Long-term outcomes of clinical complete responders after neoadjuvant treatment for rectal cancer in the international watch & wait database (Iwwd): an international multicentre registry study, Lancet 391 (10139) (2018) 2537–2545.

[4] A. Hartley, K.F. Ho, C. McConkey, J.I. Geh, Pathological complete response following pre-operative chemoradiation in rectal cancer: analysis of phase II/III trials, Br. J. Radiol. 78 (934) (2005) 934–938.

[5] Cancer.net. Colorectal Cancer: Statistics, Available at: https://www.cancer.net/cancer-types/colorectal-cancer/statistics. Accessed: February 13, 2023.

[6] M. Navarro, E. Dotor, F. Rivera, et al., A phase II study of preoperative radiotherapy and concomitant weekly irinotecan in combination with protracted venous infusion 5-fluorouracil, for resectable locally advanced rectal cancer, Int. J. Radiat. Oncol. Biol. Phys. 66 (1) (2006) 201–205.

[7] F. Willeke, K. Horisberger, U. Kraus-Tiefenbacher, et al., A phase II study of capecitabine and irinotecan in combination with concurrent pelvic radiotherapy (CapIri-RT) as neoadjuvant treatment of locally advanced rectal cancer, Br. J. Cancer 96 (6) (2007) 912–917.

[8] S.W. Gollins, S. Myint, S. Susnerwala, et al., Preoperative downstaging chemoradiation with concurrent irinotecan and capecitabine in MRI-defined locally advanced rectal cancer: a phase I trial (NWCOG-2), Br. J. Cancer 101 (6) (2009) 924–934.

[9] Y.S. Hong, D.Y. Kim, S.B. Lim, et al., Preoperative chemoradiation with irinotecan and capecitabine in patients with locally advanced resectable rectal cancer: long-term results of a Phase II study, Int. J. Radiat. Oncol. Biol. Phys. 79 (4) (2011) 1171–1178.

[10] R.D. Hofheinz, B. von Gerstenberg-Helldorf, F. Wenz, et al., Phase I trial of capecitabine and weekly irinotecan in combination with radiotherapy for neoadjuvant therapy of rectal cancer, J. Clin. Oncol. 23 (7) (2005) 1350–1357.

[11] S. Gollins, A. Sun Myint, B. Haylock, et al., Preoperative chemoradiotherapy using concurrent capecitabine and irinotecan in magnetic resonance imaging-defined locally advanced rectal cancer: impact on long-term clinical outcomes, J. Clin. Oncol. 29 (8) (2011) 1042–1049.

[12] S.J. Wong, K. Winter, N.J. Meropol, et al., Radiation Therapy Oncology Group 0247: a randomized Phase II study of neoadjuvant capecitabine and irinotecan or capecitabine and oxaliplatin with concurrent radiotherapy for patients with locally advanced rectal cancer, Int. J. Radiat. Oncol. Biol. Phys. 82 (4) (2012) 1367–1375.

[13] S.J. Wong, J. Moughan, N.J. Meropol, et al., Efficacy endpoints of radiation therapy group protocol 0247: a randomized, phase 2 study of neoadjuvant radiation therapy plus concurrent capecitabine and irinotecan or capecitabine and oxaliplatin for patients with locally advanced rectal cancer, Int. J. Radiat. Oncol. Biol. Phys. 91 (1) (2015) 116–123.

[14] K. Shulman, I. Cohen, O. Barnett-Griness, et al., Clinical implications of UGT1A1*28 genotype testing in colorectal cancer patients, Cancer 117 (14) (2011) 3156–3162.

[15] F. Innocenti, S.D. Undevia, L. Iyer, et al., Genetic variants in the UDP-glucuronosyltransferase 1A1 gene predict the risk of severe neutropenia of irinotecan, J. Clin. Oncol. 22 (8) (2004) 1382–1388.

[16] J. Zhu, A. Liu, X. Sun, et al., Multicenter, randomized, phase III trial of neoadjuvant chemoradiation with capecitabine and irinotecan guided by UGT1A1 status in patients with locally advanced rectal cancer, J. Clin. Oncol. 38 (36) (2020) 4231–4239.

[17] D.T. Le, J.N. Durham, K.N. Smith, et al., Mismatch repair deficiency predicts response of solid tumors to pd-1 blockade, Science 357 (6349) (2017) 409–413.
[18] J.M. Michael-Robinson, A. Biemer-Huttmann, D.M. Purdie, et al., Tumour infiltrating lymphocytes and apoptosis are independent features in colorectal cancer stratified according to microsatellite instability status, Gut 48 (3) (2001) 360–366.
[19] T. Andre, K.K. Shiu, T.W. Kim, et al., Pembrolizumab in microsatellite-Instability-High advanced colorectal cancer, N. Engl. J. Med. 383 (23) (2020) 2207–2218.
[20] J. Taieb, M. Svrcek, R. Cohen, et al., Deficient mismatch repair/microsatellite unstable colorectal cancer: diagnosis, prognosis and treatment, Eur. J. Cancer 175 (2022) 136–157.
[21] M. McLaughlin, E.C. Patin, M. Pedersen, et al., Inflammatory microenvironment remodelling by tumour cells after radiotherapy, Nat. Rev. Cancer 20 (4) (2020) 203–217.
[22] L. Sun, J. Wu, F. Du, et al., Cyclic GMP-AMP synthase is a cytosolic DNA sensor that activates the type I interferon pathway, Science 339 (2013) 786–791.
[23] D.L. Burdette, K.M. Monroe, K. Sotelo-Troha, et al., STING is a direct innate immune sensor of cyclic di-GMP, Nature 478 (7370) (2011) 515–518.
[24] T. Sen, B.L. Rodriguez, L. Chen, et al., Targeting DNA damage response promotes antitumor immunity through STING-mediated T-cell activation in small cell lung cancer, Cancer Discov. 9 (5) (2019) 646–661.
[25] Z. Wang, J. Chen, J. Hu, et al., cGAS/STING axis mediates a topoisomerase II inhibitor-induced tumor immunogenicity, J. Clin. Invest. 129 (11) (2019) 4850–4862.
[26] X. Liu, J. Jiang, R. Chan, et al., Improved efficacy and reduced toxicity using a custom-designed irinotecan-delivering silicasome for orthotopic colon cancer, ACS Nano 13 (1) (2019) 38–53.
[27] X. Liu, J. Jiang, Y.P. Liao, et al., Combination chemo-immunotherapy for pancreatic cancer using the immunogenic effects of an irinotecan silicasome nanocarrier plus anti-PD-1, Adv. Sci. 8 (6) (2021) 2002147.
[28] T. Yamazaki, K.H. Young, Effects of radiation on tumor vasculature, Mol. Carcinog. 61 (2) (2022) 165–172.
[29] J.M. Price, A. Prabhakaran, C.M.L. West, Predicting tumour radiosensitivity to deliver precision radiation, Nat. Rev. Clin. Oncol. 20 (2) (2023) 83–98.
[30] T. Ubhi, G.W. Brown, Exploiting DNA replication stress for cancer treatment, Cancer Res. 79 (8) (2019) 1730–1739.
[31] U.S. Srinivas, B.W.Q. Tan, B.A. Vellayappan, A.D. Jeyasekharan, ROS and the DNA damage response in cancer, Redox Biol. 25 (2019), 101084.
[32] A. Ianevski, A.K. Giri, T. Aittokallio, SynergyFinder 2.0: visual analytics of multi-drug combination synergies, Nucleic Acids Res. 48 (W1) (2020) W488–W493.
[33] Q. Liu, X. Yin, L.R. Languino, D.C. Altieri, Evaluation of drug combination effect using a Bliss independence dose-response surface model, Stat. Biopharm. Res. 10 (2) (2018) 112–122.
[34] R.M. Chabanon, M. Rouanne, C.J. Lord, et al., Targeting the DNA damage response in immuno-oncology: developments and opportunities, Nat. Rev. Cancer (2021) 701–717.
[35] N. Samson, A. Ablasser, The cGAS-STING pathway and cancer, Nat. Can. (Ott.) 3 (12) (2022) 1452–1463.
[36] K. Crasta, N.J. Ganem, R. Dagher, et al., DNA breaks and chromosome pulverization from errors in mitosis, Nature 482 (7383) (2012) 53–58.
[37] Z. Wang, J. Chen, J. Hu, et al., cGAS/STING axis mediates a topoisomerase II inhibitor-induced tumor immunogenicity, J. Clin. Invest. 129 (11) (2019) 4850–4862.
[38] A. Kalbasi, M. Tariveranmoshabad, K. Hakimi, et al., Uncoupling interferon signaling and antigen presentation to overcome immunotherapy resistance due to JAK1 loss in melanoma, Sci. Transl. Med. 12 (565) (2020), eabb0152.
[39] A. Derer, M. Spiljar, M. Bäumler, M. Hecht, R. Fietkau, B. Frey, U.S. Gaipl, Chemoradiation increases PD-L1 expression in certain melanoma and glioblastoma cells, Front. Immunol. 7 (2016) 610.
[40] T. Iwai, M. Sugimoto, D. Wakita, et al., Topoisomerase I inhibitor, irinotecan, depletes regulatory T cells and up-regulates MHC class I and PD-L1 expression, resulting in a supra-additive antitumor effect when combined with anti-PD-L1 antibodies, Oncotarget 9 (59) (2018) 31411–31421.
[41] Y.C. Perng, D.J. Lenschow, ISG15 in antiviral immunity and beyond, Nat. Rev. Microbiol. 16 (7) (2018) 423–439.
[42] G.M. Rodriguez, D. Bobbala, D. Serrano, et al., NLRC5 elicits antitumor immunity by enhancing processing and presentation of tumor antigens to CD8(+) T lymphocytes, OncoImmunology (2016), e1151593.
[43] T.B. Meissner, A. Li, A. Biswas, et al., NLR family member NLRC5 is a transcriptional regulator of MHC class I genes, Proc. Natl. Acad. Sci. U.S.A. (2010) 13794–13799.
[44] G. Garrido, B. Schrand, A. Rabasa, et al., Tumor-targeted silencing of the peptide transporter TAP induces potent antitumor immunity, Nat. Commun. 10 (1) (2019) 3773.
[45] D.C. Drummond, C.O. Noble, Z. Guo, et al., Development of a highly active nanoliposomal irinotecan using a novel intraliposomal stabilization strategy, Cancer Res. 66 (6) (2006) 3271–3277.
[46] X. Liu, A. Situ, Y. Kang, et al., Irinotecan delivery by lipid-coated mesoporous silica nanoparticles shows improved efficacy and safety over liposomes for pancreatic cancer, ACS Nano 10 (2) (2016) 2702–2715.
[47] X. Liu, P. Lin, I. Perrett, et al., Tumor-penetrating peptide enhances transcytosis of silicasome-based chemotherapy for pancreatic cancer, J. Clin. Invest. 127 (5) (2017) 2007–2018.
[48] C. Vanpouille-Box, A. Alard, M.J. Aryankalayil, et al., DNA exonuclease Trex1 regulates radiotherapy-induced tumour immunogenicity, Nat. Commun. 8 (2017), 15618.
[49] Z.J. Long, J.D. Wang, J.Q. Xu, et al., cGAS/STING cross-talks with cell cycle and potentiates cancer immunotherapy, Mol. Ther. 30 (3) (2022) 1006–1017.
[50] A. Wang-Gillam, C.P. Li, G. Bodoky, et al., Nanoliposomal irinotecan with fluorouracil and folinic acid in metastatic pancreatic cancer after previous gemcitabine-based therapy (NAPOLI-1): a global, randomised, open-label, 59phase 3 trial, Lancet 387 (10018) (2016) 545–557.
[51] B. Chibaudel, F. Maindrault-Gœbel, J.B. Bachet, et al., PEPCOL: a GERCOR randomized phase II study of nanoliposomal irinotecan PEP02 (MM-398) or irinotecan with leucovorin/5-fluorouracil as second-line therapy in metastatic colorectal cancer, Cancer Med. 5 (4) (2016) 676–683.
[52] S.D. Allen, X. Liu, J. Jiang, et al., Immune checkpoint inhibition in syngeneic mouse cancer models by a silicasome nanocarrier delivering a GSK3 inhibitor, Biomaterials 269 (2021), 120635.
[53] Y. Ji, X. Liu, J. Li, et al., Use of ratiometrically designed nanocarrier targeting CDK4/6 and autophagy pathways for effective pancreatic cancer treatment, Nat. Commun. 11 (1) (2020) 4249.
[54] X. Liu, I. Tang, Z.A. Wainberg, H. Meng, Safety considerations of cancer nanomedicine-A Key step toward translation, Small 16 (36) (2020), e2000673.
[55] X. Liu, H. Meng, Consideration for the scale-up manufacture of nanotherapeutics-A critical step for technology transfer, View 2 (2021), 20200190.
[56] P.N. Kouam, G.A. Rezniczek, I.A. Adamietz, H. Buhler, Ionizing radiation increases the endothelial permeability and the transendothelial migration of tumor cells through ADAM10-activation and subsequent degradation of VE-cadherin, BMC Cancer 19 (1) (2019) 958.
[57] S. Kabacik, K. Raj, Ionising radiation increases permeability of endothelium through ADAM10-mediated cleavage of VE-cadherin, Oncotarget 8 (47) (2017) 82049–82063.
[58] G. Pépin, C. Nejad, J. Ferrand, B.J. Thomas, H.J. Stunden, E. Sanij, C.H. Foo, C. R. Stewart, J.E. Cain, P.G. Bardin, B.R.G. Williams, M.P. Gantier, Topoisomerase 1 inhibition promotes cyclic GMP-AMP synthase-dependent antiviral responses, mBio 8 (5) (2017), e01611-e01617.
[59] J. Marinello, A. Arleo, M. Russo, et al., Topoisomerase I poison-triggered immune gene activation is markedly reduced in human small-cell lung cancers by impairment of the cGAS/STING pathway, Br. J. Cancer 127 (7) (2022) 1214–1225.
[60] C. Vanpouille-Box, A. Alard, M.J. Aryankalayil, et al., DNA exonuclease Trex1 regulates radiotherapy-induced tumour immunogenicity, Nat. Commun. 8 (2017), 15618.
[61] S.M. Harding, J.L. Benci, J. Irianto, et al., Mitotic progression following DNA damage enables pattern recognition within micronuclei, Nature 548 (7668) (2017) 466–470.
[62] T. Yamazaki, K.H. Young, Effects of radiation on tumor vasculature, Mol. Carcinog. 61 (2) (2022) 165–172.
[63] Y. Zhang, M. Huo, J. Zhou, Xie S. Pksolver, An add-in program for pharmacokinetic and pharmacodynamic data analysis in microsoft excel, Comput. Methods Progr. Biomed. 99 (2010) 306–314.